

LETTER TO THE EDITOR

Episodic modulations in supernova radio light curves from luminous blue variable supernova progenitor models

Takashi J. Moriya^{1,2,3}, Jose H. Groh⁴, and Georges Meynet⁴

¹ Kavli Institute for the Physics and Mathematics of the Universe (WPI), Todai Institutes for Advanced Study, University of Tokyo, Kashiwanoha 5-1-5, Kashiwa, Chiba 277-8583, Japan; e-mail: takashi.moriya@ipmu.jp

² Department of Astronomy, Graduate School of Science, University of Tokyo, Hongo 7-3-1, Bunkyo, Tokyo, Japan

³ Research Center for the Early Universe, Graduate School of Science, University of Tokyo, Hongo 7-3-1, Bunkyo, Tokyo, Japan

⁴ Geneva Observatory, Geneva University, Chemin des Maillettes 51, 1290 Sauverny, Switzerland

ABSTRACT

Context. Ideally, one would like to know which type of core-collapse supernovae (SNe) is produced by different progenitors and the channels of stellar evolution leading to these progenitors. These links have to be very well known to use the observed frequency of different types of SN events for probing the star formation rate and massive star evolution in different types of galaxies.

Aims. We investigate the link between luminous blue variable (LBV) as SN progenitors and the appearance of episodic light curve modulations in the radio light curves of the SN event.

Methods. We use the $20 M_{\odot}$ and $25 M_{\odot}$ models with rotation at solar metallicity, part of an extended grid of stellar models computed by the Geneva team. At their pre-SN stage, these two models have recently been shown to have spectra similar to those of LBV stars and possibly explode as Type IIb SNe. Based on the wind properties before the explosion, we derive the density structure of their circumstellar medium. This structure is used as input for computing the SN radio light curve.

Results. We find that the $20 M_{\odot}$ model shows radio light curves with episodic luminosity modulations, similar to those observed in some Type IIb SNe. This occurs because the evolution of the $20 M_{\odot}$ model terminates in a region of the HR diagram where radiative stellar winds present strong density variations, caused by the bistability limit. The $25 M_{\odot}$ model, ending its evolution in a zone of the HR diagram where no change of the mass-loss rates is expected, presents no such modulations in its radio SN light curve.

Conclusions. Our results reinforce the link between SN progenitors and LBV stars. We also confirm the existence of a physical mechanism for a single star to have episodic radio light curve modulations. In the case of the $25 M_{\odot}$ progenitors, we do not obtain modulations in the radio light curve, but our models may miss some outbursting behavior in the late stages of massive stars.

Key words. circumstellar matter – mass-loss – supernovae: general – supernovae: individual: SN 2001ig, SN 2003bg

1. Introduction

In the past decade, supernova (SN) progenitor surveys using pre-explosion images have revealed the properties of massive stars shortly before the explosions (Smartt 2009 for a review). Some SN progenitors have been linked to luminous blue variables (LBVs) (e.g., Kotak & Vink 2006; Smith et al. 2007; Gal-Yam & Leonard 2009; Moriya et al. 2013; Mauerhan et al. 2013). However, until recently, LBVs were theoretically considered to be at the transitional phase to Wolf-Rayet stars and their core does not collapse at this stage (e.g., Maeder & Meynet 2000a; Langer 2012). Recently, Groh et al. (2013) showed that the theoretical spectra of the rotating $20 M_{\odot}$ and $25 M_{\odot}$ pre-SN models are similar to those of LBVs, and that some SN progenitors can be at the LBV stage at the time of the core-collapse explosion. These models have also been suggested to explode as Type IIb SNe (SNe IIb) (Groh et al. 2013).

The possibility of LBVs being SN progenitors has been originally suggested by Kotak & Vink (2006, KV06 hereafter) through the interpretation of SN radio light curves (LCs). Radio emission from SNe is caused by the interaction between SN ejecta and the progenitors' circumstellar media (CSM). Therefore, the mass-loss history of the SN progenitor is imprinted in SN radio LCs (e.g., Weiler et al. 2002; Chevalier et al.

2006; Chevalier & Fransson 2006). Radio emission from some SNe is known to have episodic luminosity enhancements, as has been clearly observed in, e.g., SN IIb 2001ig (Ryder et al. 2004), SN IIb 2003bg (Soderberg et al. 2006), SN IIb 2008ax (Roming et al. 2009), SN IIb 2011ei (Milisavljevic et al. 2013), SN Ic 1998bw (Kulkarni et al. 1998), and SN IIL 1979C (Weiler et al. 1992). KV06 suggested that the timescales of the episodic radio modulations are consistent with S Doradus-type mass loss, which occurs only in LBVs. During the S Doradus variability, the star crosses the bistability limit, in which the mass-loss rate (\dot{M}) and wind terminal velocity (v_{∞}) change abruptly (e.g. Groh et al. 2009, 2011; Groh & Vink 2011). The changes are regulated by Fe recombination in the inner wind, leading to changes in the wind driving and thus in \dot{M} and v_{∞} (Pauldrach & Puls 1990; Vink et al. 1999; Vink & de Koter 2002). A density change by a factor of $\sim 4 - 10$ would be expected, and this recurrent behavior would create an inhomogeneous CSM around the LBV at the pre-SN stage, causing the observed radio LC variations (KV06).

In this Letter, we investigate the behavior of the 20 and $25 M_{\odot}$ LBV models centuries before their explosions. We show that the $20 M_{\odot}$ SN progenitor model flirts with the bistability limit, presenting variable mass loss and an inhomogeneous CSM density structure at the time of the explosion. We present a quanti-

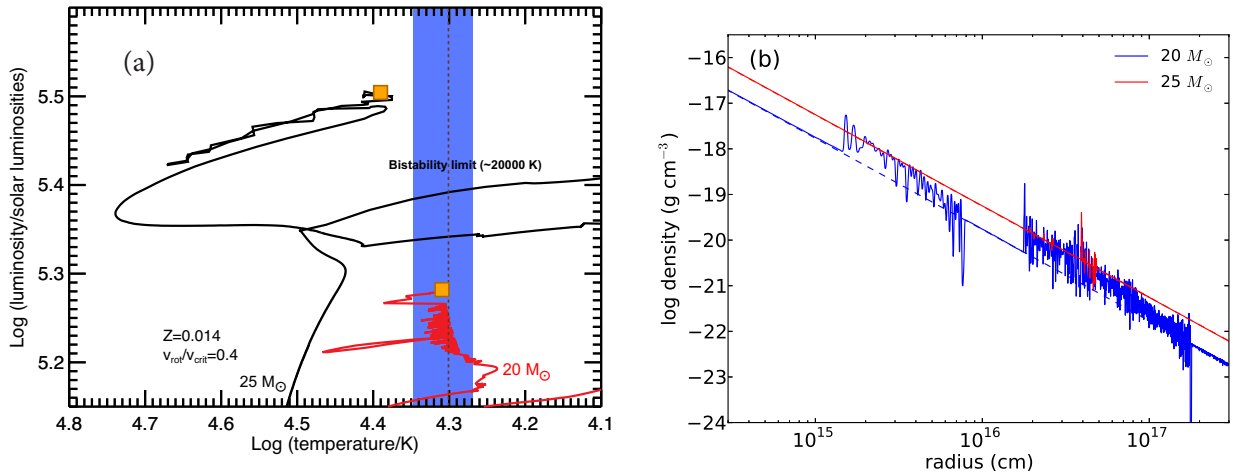


Fig. 1. (a) End part of the evolutionary tracks in the HR diagram for the 20 and 25 M_{\odot} rotating models. The end point is shown as an orange square. The bistability limit, where jumps in \dot{M} and v_{∞} occur, is indicated in blue. The vertical line corresponds to the bistability limit computed for the end point according to the Vink et al. (1999) recipe. (b) CSM density structures obtained from the evolutionary models (solid lines). The CSM densities with dashed lines are the CSM without the mass loss variations and used to obtain the reference LCs.

tative model for the SN radio LC that can naturally explain the episodic radio LC modulations from the single-star evolutionary point of view. Our results bring further support to the idea that a fraction of LBVs can be the end stage of massive stars.

2. Stellar Evolution

2.1. Pre-Supernova Models at the LBV Phase

The 20 and 25 M_{\odot} stellar models discussed here have been computed by Ekström et al. (2012) for an initial metallicity $Z = 0.014$. The physical ingredients used to compute these models can be found in this reference as well as a presentation of their main characteristics. Let us just recall here a few points allowing to make the present paper self-explanatory. The time averaged equatorial rotation velocities during the main-sequence phase are equal to 217 (20 M_{\odot}) and 209 km s^{-1} (25 M_{\odot}). An overshooting equal to 10% of the pressure scale at the border of the Schwarzschild convective core has been accounted for. The radiative mass-loss rate adopted is from Vink et al. (2001). In the domains not covered by this prescription, we use de Jager et al. (1988). We have applied a correction factor due to rotation to the radiative mass-loss rate as described in Maeder & Meynet (2000b). For the two models discussed here, this correcting factor has very little impact on the mass-loss rates. In the red supergiant (RSG) phase, when some of the most external layers of the stellar envelope exceed the Eddington luminosity of the star, the mass-loss rate of the star (computed according to the prescription described above) is increased by a factor of 3. As emphasized by Ekström et al. (2012), this prescription gives \dot{M} during the RSG phase compatible with those of RSGs obtained by van Loon et al. (2005).

These two models end their nuclear lifetimes in the blue part of the HR diagram (Fig. 1a). Groh et al. (2013) showed that the spectrum of these stars at the pre-SN stage looks like quiescent LBV stars, showing for the first time that single star evolution may produce LBV-type progenitors of core-collapse SN events. Interestingly, Fig. 1a shows that the 20 M_{\odot} model ends its evolution when its surface conditions are just at the frontier between two regimes of mass loss that characterizes the bistability limit, as described above. On the basis of mass-loss properties, Vink & de Koter (2002) proposed a connection between

the bistability limit and the LBV stars. Here we show from a stellar evolution point of view that indeed there may be such a connection.

From Fig. 1a, we see that our 20 M_{\odot} model has the effective temperatures at the end of its evolution which oscillate around $\log(T_{\text{eff}}/\text{K}) = 4.3$, implying variations of the mass-loss rates between about 1.2×10^{-5} (on the hot side of the bistability limit) and $15 \times 10^{-5} M_{\odot} \text{ yr}^{-1}$ (on the cool side). Thus this model would nicely fit the picture described in Vink et al. (1999); Vink & de Koter (2002). On the other hand, in the case of our 25 M_{\odot} model, the end point is at a too high effective temperature for such a process to occur. Actually, both models could present another type of mass-loss variability before they explode. For example, S Doradus variability could still occur and produce variable \dot{M} near the end stage. Unfortunately, at the moment there is no accepted theory to explain the S Doradus variability, so they cannot be self-consistently included in the evolutionary models.

We have thus two models presenting an LBV-type spectrum at the pre-SN stage. One, the 20 M_{\odot} model, just stops in the vicinity of the bistability limit while the other has its end point far from this limit. Let us now study the consequences of these two types of behavior on the SN radio LCs. For this purpose, we need first to derive the CSM properties of the pre-SN stars.

2.2. Circumstellar Media

To construct the CSM density structures from the mass-loss rates and the wind velocities obtained by the stellar evolutionary model, we perform one-dimensional spherically-symmetric numerical hydrodynamics calculations with ZEUS-MP2 version 2.1.2 (Hayes et al. 2006). The CSM structures of the region between $1.5 \times 10^{13} \text{ cm}$ ($6R_{\star}$, where R_{\star} is the stellar radius of the 20 M_{\odot} model) and $3 \times 10^{17} \text{ cm}$ ($10^5 R_{\star}$) are followed by setting the inner boundary conditions at $1.5 \times 10^{13} \text{ cm}$ based on the mass-loss rates and wind velocities.

The CSM density structures obtained are shown in Fig. 1b. In the 20 M_{\odot} model, there exist two extended high-density regions. The two regions correspond to the two enhanced mass-loss periods caused by the star crossing to the cool side of the bistability limit. The small-scale density variations are due to

the rapid variations in the mass-loss rate. On the contrary, the $25 M_{\odot}$ model does not have significant variations in the mass-loss rate shortly before the core collapse and it does not have any extended high-density regions in the CSM near the progenitor.

3. Supernova Radio Light Curve

3.1. Radio Light Curve Model

We calculate SN radio LCs based on the CSM density structures obtained in Section 2.2. SN radio emission is considered to be synchrotron emission from the accelerated electrons at the forward shock. We obtain the synchrotron luminosity by following the formalism developed by Fransson & Björnsson (1998); Björnsson & Fransson (2004) (see also Maeda 2012). The synchrotron luminosity L_{ν} at a frequency ν is approximated as

$$\nu L_{\nu} \approx \pi R_{\text{sh}}^2 V_{\text{sh}} n_{\text{rel}} \left(\frac{\gamma_{\nu}}{\gamma_{\text{min}}} \right)^{1-p} \gamma_{\nu} m_e c^2 \left[1 + \frac{t_{\text{sync}}(\nu)}{t} \right]^{-1}, \quad (1)$$

where m_e is the electron mass and c is the speed of light. R_{sh} and V_{sh} are the radius and the velocity of the forward shock, respectively. n_{rel} is the number density of the relativistic electrons. We set the distribution of the relativistic electrons as $dn_{\text{rel}}(\gamma)/d\gamma \propto \gamma^{-p}$ where γ is the Lorentz factor. We adopt $p = 3$, which is the canonical value for the synchrotron emission from SNe. γ_{min} is the minimum Lorentz factor of the accelerated electrons and usually assumed to be $\gamma_{\text{min}} \sim 1$. $\gamma_{\nu} = (2\pi m_e c \nu / eB)^{0.5}$, where e is the electron charge and B is the magnetic field strength, is the Lorentz factor of electrons emitting at the characteristic frequency ν . $t_{\text{sync}}(\nu) = 6\pi m_e c / \sigma_T \gamma_{\nu} B^2$ is the cooling timescale of electrons emitting at ν by the synchrotron cooling, where σ_T is the Thomson cross section. In addition, we take the synchrotron self-absorption (SSA) into account (e.g., Chevalier 1998). Free-free absorption is ignored because of the low CSM density. We use the SSA optical depth $\tau_{\text{SSA}} = (\nu/\nu_{\text{SSA}})^{-(p+4)/2}$. For $p = 3$, the SSA frequency ν_{SSA} is $\approx 3 \times 10^5 (R_{\text{sh}} \epsilon_e / \epsilon_B)^{2/7} B^{9/7}$ Hz in cgs units, where ϵ_e is the fraction of thermal energy in the shock used for the electron acceleration and ϵ_B is the fraction converted to the magnetic field energy.

We adopt the self-similar solution of Chevalier (1982) for R_{sh} and V_{sh} . The SN ejecta with kinetic energy E_{ej} and mass M_{ej} is assumed to have the density structure with the two power-law components ($\rho \propto r^{-n}$ outside and $\rho \propto r^{-\delta}$ inside). We adopt $n = 10.2$ and $\delta = 1.1$ which approximate the numerical explosion of SN Iib/Ib/Ic progenitors (Matzner & McKee 1999). For simplicity, we ignore the effect of the density jumps in CSM on R_{sh} and V_{sh} as is also assumed in Soderberg et al. (2006). We use the dashed density structures in Fig. 1b to obtain R_{sh} and V_{sh} . We constrain M_{ej} by subtracting the remnant mass $1.4 M_{\odot}$ from the progenitor mass obtained by Ekström et al. (2012) and $M_{\text{ej}} = 5.7 M_{\odot}$ ($20 M_{\odot}$ model) and $M_{\text{ej}} = 8.2 M_{\odot}$ ($25 M_{\odot}$ model).

3.2. Results

SN radio LCs obtained from the $20 M_{\odot}$ LBV SN progenitor exploded with the standard SN ejecta kinetic energy $E_{\text{ej}} = 10^{51}$ erg are presented in Fig. 2. We assume $\epsilon_e = 0.1$ and $\epsilon_B = 0.1$ here. The radio LCs show two episodic modulations. They result from the two high-density regions due to the mass-loss enhancements caused by the bistability limit shortly before the explosion. The forward shock reaches the first high-density region at around 8 days since the explosion. At this time, the effect of the SSA is still dominant at 1.43 GHz, 4.86 GHz, and 8.46 GHz and the radio luminosities at these frequencies decrease due to the density

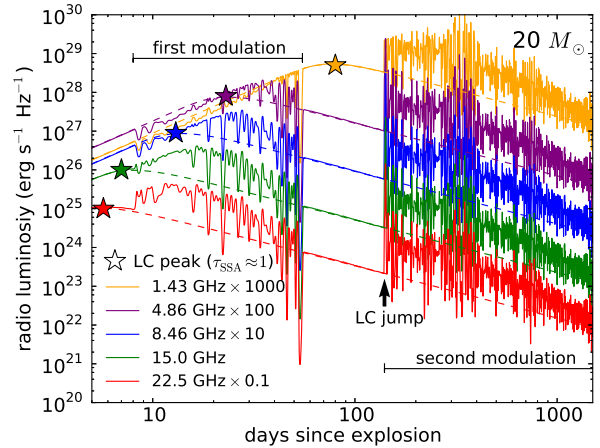


Fig. 2. Synthesized radio LCs with the standard SN kinetic energy $E_{\text{ej}} = 10^{51}$ erg from the $20 M_{\odot}$ model (solid lines). The reference LCs without the CSM density variations are also shown (dashed lines, see Fig. 1b). The star symbols indicate the LC peaks of the reference LCs.

enhancement. As time passes, the SSA gets less effective and the radio luminosities start to be enhanced by the density increase. At the time when the forward shock reaches the second high-density region at around 140 days, the SSA is negligible in all the frequencies in Fig. 2 and the radio luminosities are enhanced by about a factor 5 on average in all the bands. The radio LCs also have very short variations which are caused by the small-scale density variations seen in Fig. 1b. However, these short-time variations should be smoothed by the light-travel-time delays caused by the large emitting radii which are not taken into account in our modeling. On the contrary, the $25 M_{\odot}$ model does not show the LC modulations as its surface temperature is far from from the temperature of the bistability limit and there is no significant mass-loss increase shortly before the explosion.

To detect the overall features of the radio LCs caused by the LBV progenitor predicted here in Fig. 2, we need to be sensitive to the radio luminosity of $\sim 10^{24}$ erg s $^{-1}$ Hz $^{-1}$. Using the Extended Very Large Array, which is sensitive down to $\sim 1 \mu\text{Jy}$ (Perley et al. 2011), the predicted SN radio LC features can be observed if the corresponding SN appears within 30 Mpc.

4. Comparison with Observations

The inhomogeneous density structure around our model progenitors is reminiscent of that qualitatively proposed by KV06 to explain the episodic modulations in the radio LCs of some SNe. Let us now compare our models with the observations. We compare our $20 M_{\odot}$ model with SNe Iib 2001ig (Ryder et al. 2004) and 2003bg (Soderberg et al. 2006). Their radio luminosities are higher than those we obtained in the previous section. The radio luminosities (Eq. 1) follow

$$L_{\nu} \propto \epsilon_e \epsilon_B^{\frac{p+1}{4}} E_{\text{ej}}^{\frac{3(n-3)}{2(n-2)}} M_{\text{ej}}^{-\frac{3(n-5)}{2(n-2)}} \left(\frac{\dot{M}}{v_{\infty}} \right)^{\frac{p+5}{4} - \frac{3}{n-2}} \approx \epsilon_e \epsilon_B E_{\text{ej}}^{1.3} M_{\text{ej}}^{-0.95} \left(\frac{\dot{M}}{v_{\infty}} \right)^{1.6}. \quad (2)$$

The right-hand side of Eq. 2 is for $p = 3$ and $n = 10.2$. In this section, we show that the observed SN Iib radio LCs can be explained by our model just by slightly changing the SN and predicted CSM properties.

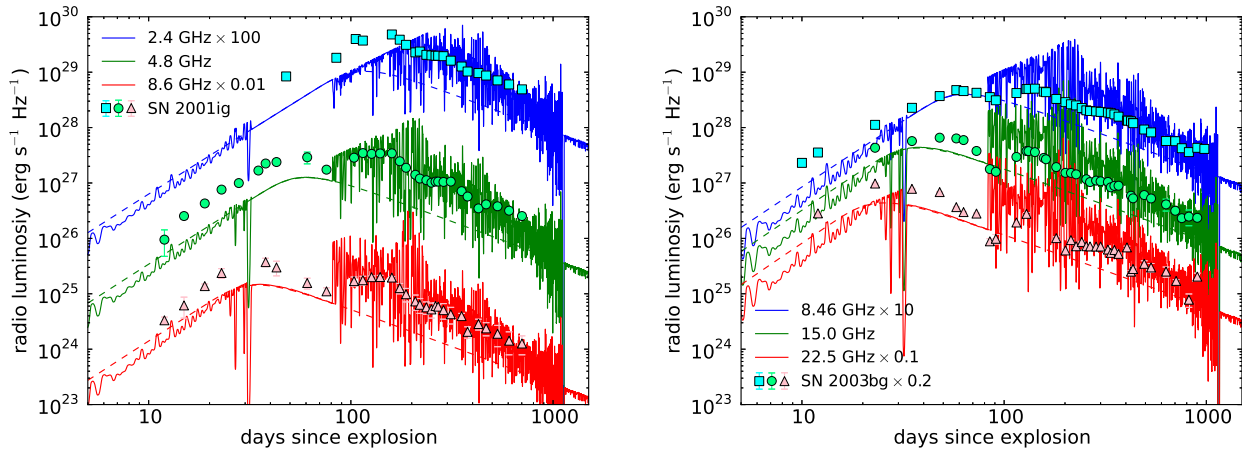


Fig. 3. Comparisons between the model radio LCs from the $20 M_{\odot}$ model and the observed radio LCs of SNe Iib 2001ig (Ryder et al. 2004) and 2003bg (Soderberg et al. 2006). The frequencies of the observed radio LCs are 2.4 GHz (square), 4.8 GHz (circle), and 8.6 GHz (triangle) in the left panel. The LCs of 2.4 GHz and 8.6 GHz are multiplied by 100 and 0.01, respectively, for the illustrative purpose. In the right panel, the frequencies of the observed radio LCs are 8.46 GHz (square), 15.0 GHz (circle), and 22.5 GHz (triangle). The LCs of 8.46 GHz and 22.5 GHz are multiplied by 10 and 0.1, respectively. The radio LCs of SN 2003bg are multiplied by 0.2 additionally to match the synthesized LCs.

In Fig. 3, we show the results of the comparisons. On the left panel, our radio LC model is compared with SN Iib 2001ig. To match the observed LCs, the CSM density is increased by a factor 3 and we set $E_{ej} = 4 \times 10^{51}$ erg. In addition, to adjust the time of the LC peak before the second LC modulation, we set $\epsilon_e = 0.2$ and $\epsilon_B = 0.08$ (see τ_{SSA} in Section 3.1). We can see that the radio LC features of SN 2001ig are reproduced well by the above parameters which are not so different from those of the standard model we presented in Section 3. The episodic radio LC jump observed at around 100 days matches the epoch when the model LCs start to show the second modulation. This shows that the changes in the CSM density that occur because of the crossing of the bistability limit are able to explain the modulation in the SN radio LC. The amount of the observed radio luminosity increase also matches that in our model. This quantitative finding reinforces the link between LBVs as SN progenitors and the modulations in their radio LCs. In addition, it strengthens the idea that part of the SN Iib progenitors can be LBVs (KV06, Groh et al. 2013). We confirm the existence of a physical mechanism for a single star to make the inhomogeneous CSM around the SN 2001ig progenitor which has often been related to the binary evolution (Ryder et al. 2004, 2006).

The right panel shows the comparison with SN 2003bg. The CSM density is increased by a factor 8 and $E_{ej} = 5 \times 10^{51}$ erg in the model shown. We keep $\epsilon_e = 0.2$ and $\epsilon_B = 0.08$. The overall features of the observed LCs are reproduced. However, the absolute luminosities of SN 2003bg are still higher than those of the model, so the observations are scaled to match the model. We can increase the luminosity by increasing E_{ej} but this makes the time of the LC jump much earlier than the observed time. This indicates that there is a diversity in the time of the mass-loss variations due to the bistability limit, which is naturally expected.

The currently best observed SN Iib in radio is SN 1993J (e.g., Weiler et al. 2007). It does not show the episodic LC modulations we present here but the progenitor is suggested to have had a sharp increase in the mass-loss rate at around 10^4 years before the explosion (Weiler et al. 2007). Therefore, the timing of the mass-loss variation may be crucial for observing episodic modulations in SN radio LCs.

We also note that the epochs of the first episodic luminosity decrease/increase in the model was not covered by the observations well. Observing these early modulations has the potential to probe mass loss immediately before the SN explosion, so early radio observations of SNe would be extremely invaluable.

Acknowledgements. We thank the referee for valuable comments. T.J.M. thanks Keiichi Maeda for useful discussion. Numerical computations were in part carried out on the general-purpose PC farm at Center for Computational Astrophysics, National Astronomical Observatory of Japan. T.J.M. is supported by the Japan Society for the Promotion of Science Research Fellowship for Young Scientists (23-5929). This work is also supported by World Premier International Research Center Initiative (WPI Initiative), MEXT, Japan. J.H.G. is supported by an Ambizione Fellowship of the Swiss National Science Foundation.

References

- Björnsson, C.-I., & Fransson, C. 2004, *ApJ*, 605, 823
 Chevalier, R. A. 1998, *ApJ*, 499, 810
 Chevalier, R. A. 1982, *ApJ*, 258, 790
 Chevalier, R. A., & Fransson, C. 2006, *ApJ*, 651, 381
 Chevalier, R. A., Fransson, C., & Nymark, T. K. 2006, *ApJ*, 641, 1029
 de Jager, C., Nieuwenhuijzen, H., & van der Hucht, K. A. 1988, *A&AS*, 72, 259
 Ekström, S., Georgy, C., Eggenberger, P., et al. 2012, *A&A*, 537, A146
 Gal-Yam, A., & Leonard, D. C. 2009, *Nature*, 458, 865
 Groh, J. H., Hillier, D. J., Damineli, A., et al. 2009, *ApJ*, 698, 1698
 Groh, J. H., Hillier, D. J., & Damineli, A. 2011, *ApJ*, 736, 46
 Groh, J. H. & Vink, J. S. 2011, *A&A*, 531, L10
 Groh, J. H., Meynet, G., & Ekström, S. 2013, *A&A*, 550, L7
 Fransson, C., & Björnsson, C.-I. 1998, *ApJ*, 509, 861
 Hayes, J. C., Norman, M. L., Fiedler, R. A., et al. 2006, *ApJS*, 165, 188
 Kotak, R., & Vink, J. S. 2006, *A&A*, 460, L5 (KV06)
 Kulkarni, S. R., Frail, D. A., Wieringa, M. H., et al. 1998, *Nature*, 395, 663
 Langer, N. 2012, *ARA&A*, 50, 107
 Maeda, K. 2012, *ApJ*, 758, 81
 Maeder, A., & Meynet, G. 2000a, *ARA&A*, 38, 143
 Maeder, A., & Meynet, G. 2000b, *A&A*, 361, 159
 Matzner, C. D., & McKee, C. F. 1999, *ApJ*, 510, 379
 Mauerhan, J. C., Smith, N., Filippenko, A. V., et al. 2013, *MNRAS*, 430, 1801
 Milisavljevic, D., Margutti, R., Soderberg, A. M., et al. 2013, *ApJ*, 767, 71
 Moriya, T. J., Blinnikov, S. I., Tominaga, N., et al. 2013, *MNRAS*, 428, 1020
 Pauldrach, A. W. A. & Puls, J. 1990, *A&A*, 237, 409
 Perley, R. A., Chandler, C. J., Butler, B. J., & Wrobel, J. M. 2011, *ApJ*, 739, L1
 Roming, P. W. A., Pritchard, T. A., Brown, P. J., et al. 2009, *ApJ*, 704, L118
 Ryder, S. D., Murrowood, C. E., & Stathakis, R. A. 2006, *MNRAS*, 369, L32
 Ryder, S. D., Sadler, E. M., Subrahmanyan, R., et al. 2004, *MNRAS*, 349, 1093
 Smartt, S. J. 2009, *ARA&A*, 47, 63
 Smith, N., Li, W., Foley, R. J., et al. 2007, *ApJ*, 666, 1116

- Soderberg, A. M., Chevalier, R. A., Kulkarni, S. R., & Frail, D. A. 2006, *ApJ*, 651, 1005
- van Loon, J. T., Marshall, J. R., & Zijlstra, A. A. 2005, *A&A*, 442, 597
- Vink, J. S., de Koter, A., & Lamers, H. J. G. L. M. 1999, *A&A*, 350, 181
- Vink, J. S., de Koter, A., & Lamers, H. J. G. L. M. 2001, *A&A*, 369, 574
- Vink, J. S. & de Koter, A. 2002, *A&A*, 393, 543
- Weiler, K. W., Panagia, N., Montes, M. J., & Sramek, R. A. 2002, *ARA&A*, 40, 387
- Weiler, K. W., van Dyk, S. D., Pringle, J. E., & Panagia, N. 1992, *ApJ*, 399, 672
- Weiler, K. W., Williams, C. L., Panagia, N., et al. 2007, *ApJ*, 671, 1959